

Solvation effects on angular distributions in $\text{H}^-(\text{NH}_3)_n$ and $\text{NH}_2^-(\text{NH}_3)_n$ photodetachment: Role of solute electronic structure

Emily R. Grumbling and Andrei Sanov^{a)}

Department of Chemistry and Biochemistry, University of Arizona, Tucson, Arizona 85721, USA

(Received 15 August 2011; accepted 28 September 2011; published online 24 October 2011)

We report 355 and 532 nm photoelectron imaging results for $\text{H}^-(\text{NH}_3)_n$ and $\text{NH}_2^-(\text{NH}_3)_n$, $n = 0-5$. The photoelectron spectra are consistent with the electrostatic picture of a charged solute (H^- or NH_2^-) solvated by n ammonia molecules. For a given number of solvent molecules, the NH_2^- core anion is stabilized more strongly than H^- , yet the photoelectron angular distributions for solvated H^- deviate more strongly from the unsolvated limit than those for solvated NH_2^- . Hence, we conclude that solvation effects on photoelectron angular distributions are dependent on the electronic structure of the anion, i.e., the type of the initial orbital of the photodetached electron, rather than merely the strength of solvation interactions. We also find evidence of photofragmentation and autodetachment of $\text{NH}_2^-(\text{NH}_3)_{2-5}$, as well as autodetachment of $\text{H}^-(\text{NH}_3)_5$, upon 532 nm excitation of these species.

© 2011 American Institute of Physics. [doi:10.1063/1.3653232]

I. INTRODUCTION

Chemical structure and dynamics are determined by the interactions of electrons in and between molecules. Photoelectron spectroscopy is a powerful probe of electronic structure, with the capacity to reveal electronic and, often, vibrational energy spacings and Franck-Condon factors.^{1,2} Negative-ion photoelectron spectroscopy provides such information about the corresponding neutral molecule, as well as its electron affinity and vertical detachment energies of the anion.²

The now-widespread technique of velocity-map³ photoelectron imaging^{4,5} yields both energy spectra and photoelectron angular distributions (PAD) in a single experiment with nearly 100% collection efficiency, including detection of low-energy electrons.^{6,7} The ease of obtaining angular distributions with respect to the polarization of the incident radiation is particularly appealing, as the PADs can reveal details of the parent electronic structure and/or photoemission dynamics.⁸⁻¹¹ Both structure and dynamics are affected by chemical environment, thus affording photoelectron spectroscopy—imaging, in particular—a prized vantage point in probing elementary reactions and effects of solvation. The focus of this paper is on solvation effects on the intrinsic electronic structure of negative ions and their photodetachment dynamics.

Solvation of negative ions may be systematically examined via experiments on a series of clusters $\text{X}^-(\text{M})_n$, where n neutral molecules (M) are electrostatically (as opposed to covalently) bound to a negative ion (X^-).^{12,13} For such species, solvation is often thought of as having a perturbative effect on the energy and electronic structure of the anion core, or “solute.” As anions are stabilized more strongly by solvation than the corresponding neutrals, addition of solvent molecules

progressively increases the gap between the ground states of the anion and its corresponding neutral, thus increasing the vertical detachment energy (VDE). If the electronic structure of the solute remains approximately preserved, the photoelectron energy spectra retain their general features, apart from a shift to smaller electron kinetic energy (eKE) and, commonly, peak broadening along a solvation series. The difference in VDE between a cluster and the bare anion is an approximate measure of the solvent stabilization of the anion, while drastic spectral changes along a solvation series may indicate chemistry or physics beyond those of electrostatic ion-solvent interactions.

The effects of solvation on the corresponding PADs are more intricate and less understood. The relationship between the symmetries of the initial (bound) and final (continuum) states is defined by the transition-dipole selection rules.^{7,14} Solid theoretical foundations have been developed for understanding the resulting angular distributions for the cases of atomic and small molecular anions,^{8,15-19} but it is less so for cluster anions. In general, PADs reflect the superposition of all allowed final states, as perhaps most apparent in atomic anion photodetachment. In that case, the photoelectron wave is composed of partial waves defined by the $\ell = \ell_i \pm 1$ selection rule, with ℓ and ℓ_i being the orbital angular momentum quantum numbers of the photoelectron and the parent atomic orbital, respectively. As the relative cross-sections of different partial waves are, in general, energy dependent,²⁰⁻²² the PADs are known to vary significantly with eKE.^{8,15,16}

Within this conceptual framework, the effects of solvation on cluster-anion PADs may be separated into several broadly defined motifs. First, the solvation-induced shift of photodetachment bands to smaller eKEs affects the relative cross-sections of the allowed partial waves, thus resulting in a change in the anisotropy of the corresponding transition. Note that this effect occurs merely due to energetic stabilization of the solute anion, without accounting for any change in the anion's intrinsic structure. Second, solvent perturbation of the

^{a)} Author to whom correspondence should be addressed. Electronic mail: sanov@u.arizona.edu.

anion's intrinsic electronic structure should logically change the *types* of partial waves allowed. Thirdly, upon departure from the parent anion, the photoelectron itself may be perturbed by interactions with the neutral solvent, in particular when its kinetic energy is in the vicinity of an anionic resonance of the solvent.

Thus, cluster-anion PADs are intricately linked to the electronic structure of the solute anion and details of the detachment process. The first of the above effects is always present, and hence comparisons between PADs for bare and solvated ions must account for any difference in eKE of the bands in question.^{23–25} The third (post-detachment) motif, manifest in the presence of electron-solvent scattering resonances, was also discussed in several recent publications.^{23–27} In this work, we address the effect of solvation-induced changes in the parent orbital symmetry (i.e., the second of the above motifs) by examining PADs for two solvation series, with the same solvent but different solutes with distinct parent orbitals.

We present photoelectron imaging results for $\text{H}^-(\text{NH}_3)_n$ and $\text{NH}_2^-(\text{NH}_3)_n$ cluster anions with $n = 0–5$, obtained at 355 and 532 nm. The photoelectron energy spectra are consistent with those previously reported by the Bowen group for 488 nm photodetachment of $\text{H}^-(\text{NH}_3)_{1–2}$ and $\text{NH}_2^-(\text{NH}_3)_{1–2}$.^{28–30} However, our spectra also include the previously unobserved $\text{NH}_2(A^2A_1) \leftarrow \text{NH}_2(X^1A_1)$ photodetachment transition, as well as signatures of autodetachment and photofragmentation in some of the larger clusters probed, suggesting the existence of metastable charge-transfer states analogous to those identified for the $\text{I}^-(\text{NH}_3)_n$, $n = 4–15$, cluster series.^{31,32} We focus our discussion on the photoelectron angular distributions for the observed direct photodetachment transitions. These results suggest that the effect of any given solvent on photodetachment anisotropies depends strongly upon the nature of the parent orbital of the solute.

II. EXPERIMENTAL APPARATUS

The experiments were performed using a pulsed negative-ion photoelectron imaging spectrometer described in detail elsewhere.³³ In brief, a neutral precursor of neat ammonia or 30% ammonia seeded in argon was expanded supersonically through a pulsed nozzle (General Valve, Inc., series 9) operated at a 50 Hz repetition rate into a vacuum chamber ($\sim 10^{-6}$ Torr base pressure, $\sim 10^{-5}$ Torr under load), where it was bombarded with a counter-propagating continuous beam of 1 keV electrons from an electron gun. Negative ions³⁴ from the resulting plasma were extracted into a Wiley-McLaren³⁵ time-of-flight mass-spectrometer by a pulsed repeller plate downstream of the nozzle.³⁶ The resulting mass-spectra contained two series of peaks, corresponding to the $\text{H}^-(\text{NH}_3)_n$ and $\text{NH}_2^-(\text{NH}_3)_n$ cluster-ion series exclusively.

Photoelectron images were obtained for each cluster anion of interest ($n = 0–5$) by intersecting a linearly polarized laser pulse with the corresponding ion packet about 15 cm upstream of the ion detector, between the electrodes of a velocity-map³ imaging assembly. Photodetachment was performed with the second (532 nm) and third (355 nm) harmonics of a nanosecond pulsed Nd:YAG laser operating at a

repetition rate of 50 kHz (Quanta Ray Lab 130–50 by Spectra Physics, Inc.). In each experiment, the laser beam was slightly focused with a 2 m focal length lens placed about 1.2 m upstream of the laser-ion interaction region, to yield laser fluences of approximately $1.3–1.6 \times 10^6$ W/cm² in the region of laser-ion overlap.

Five individual images, collected over 15,000 experimental cycles each, were obtained for each species studied at each wavelength, with the exception of $\text{H}^-(\text{NH}_3)_n$, $n = 0–3$, at 355 nm, for which only three images were collected. Three-dimensional photoelectron distributions were reconstructed from each image via inverse Abel transform using the BA-SEX program.³⁷ In the following, we present the cumulative raw images and energy spectra for each cluster species studied. The photodetachment transitions for bare H^- and NH_2^- were used for energy calibration. We also analyze the PADs determined for each set of individual images.

III. RESULTS

The cumulative photoelectron images and corresponding spectra for the $\text{H}^-(\text{NH}_3)_n$, $n = 0–5$, cluster series obtained at 355 and 532 nm are presented in Figures 1 and 2, respectively. The corresponding data for $\text{NH}_2^-(\text{NH}_3)_n$, $n = 0–5$, are shown in Figures 3 and 4. The photoelectron spectra are plotted versus electron binding energy (eBE). Peak eBEs, approximately corresponding to vertical detachment energies, are indicated (in electron-volts) in plain type next to the spectral bands assigned to direct photodetachment transitions.

The photoelectron angular distributions for selected transitions were fit using the general equation for one-photon detachment with linearly polarized light:

$$I(\theta) \propto 1 + \beta(3 \cos^2 \theta - 1)/2, \quad (1)$$

where θ is the angle with respect to light's electric field and β is the unitless anisotropy parameter that in itself characterizes the distribution. The resulting β values with one-sigma error bars are reported in italics next to the corresponding spectral peaks in Figures 1–4.

A. Photoelectron spectra for $\text{H}^-(\text{NH}_3)_n$, $n = 0–5$

Photoelectron images and spectra for $\text{H}^-(\text{NH}_3)_n$, $n = 0–5$, obtained at 355 nm are displayed in Figure 1. The $n = 0$ spectrum corresponds to photodetachment from bare H^- . Its single feature at eBE = 0.75 eV reflects removal of a 1s electron, yielding the neutral H atom in the $2S_{1/2}$ ground state.³⁸ The band width reflects the instrumental resolution at the corresponding eKE.

Photodetachment from the singly solvated ($n = 1$) species yields a similar spectral feature (labeled I) shifted to a higher eBE, along with a less intense feature (II) appearing as a shoulder on the high-eBE tail of band I and peaking at an eBE approximately 0.4 eV greater than that of the primary transition. Similar features persist through $n = 5$, shifted together and monotonically to successively higher eBEs. We shall refer to the analogous but offset transitions in the spectra for $n > 1$ as type I or type II transitions. There is some broadening of these features for $n > 0$, but we note that

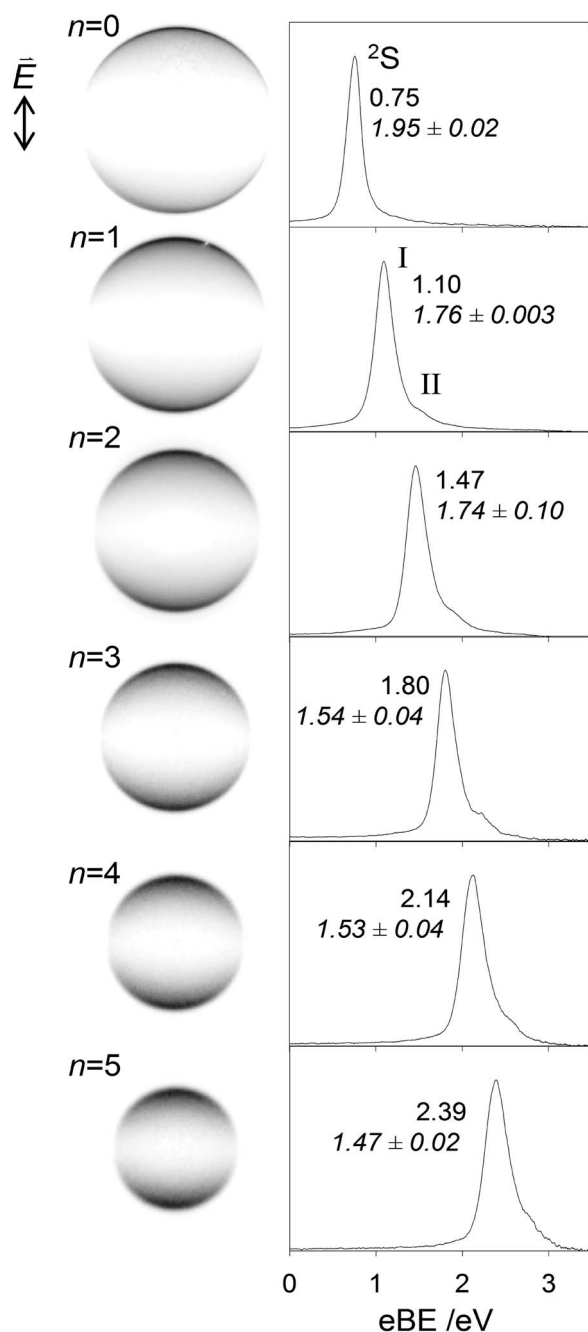


FIG. 1. Photoelectron images and energy spectra for photodetachment from $\text{H}^-(\text{NH}_3)_n$, $n = 0-5$, at 355 nm. Image intensities are arbitrarily scaled; spectra are scaled for matching peak intensities. Peak binding energies (in plain type, with ± 0.02 eV uncertainty) and anisotropy parameters (in *italics*) are indicated for the dominant transition. See text for details.

solvation-induced broadening along the series is expected to compete with improving energy resolution as n increases and eKE decreases.

Similar features were previously observed by the Bowen group for 488 nm photoelectron spectroscopy of the $n = 1-2$ species.^{28,29} We adopt their assignment of the dominant peaks (I) to direct photodetachment from H^- solvated by n ammonia molecules and the weaker feature (II) to photodetachment with activation of an asymmetric ammonia stretching mode.

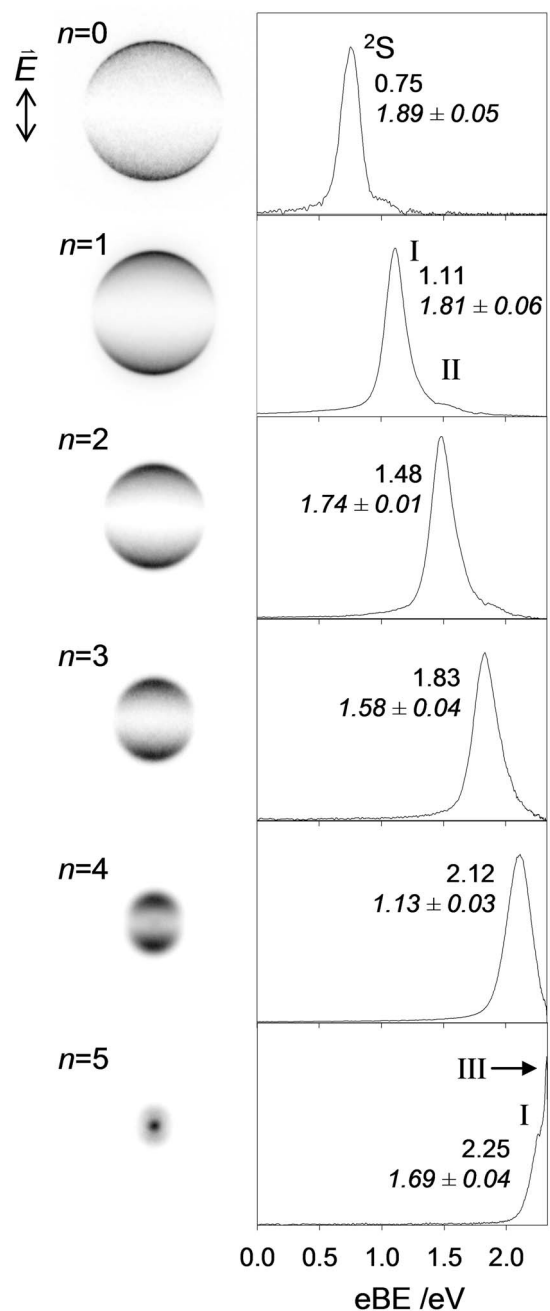


FIG. 2. Photoelectron images and energy spectra for photodetachment from $\text{H}^-(\text{NH}_3)_n$, $n = 0-5$, at 532 nm. Image intensities are arbitrarily scaled; spectra are scaled for matching peak intensities. Peak binding energies (in plain type, with ± 0.02 eV uncertainty) and anisotropy parameters (in *italics*) are indicated for the dominant transition. See text for details.

We do not observe the third peak identified by the Bowen group for $n = 1$ (with VDE = 0.472 eV) and assigned to direct photodetachment from the tetrahedral, double-Rydberg state described as $(\text{NH}_4^+)^{2-}$.

The 532 nm photoelectron images and resulting spectra for $\text{H}^-(\text{NH}_3)_n$, $n = 0-5$ are displayed in Figure 2. The spectral features are generally similar to those observed at 355 nm, but we note several differences. First, band II is not distinguishable for $n = 3$, most likely due to threshold cross-sectional

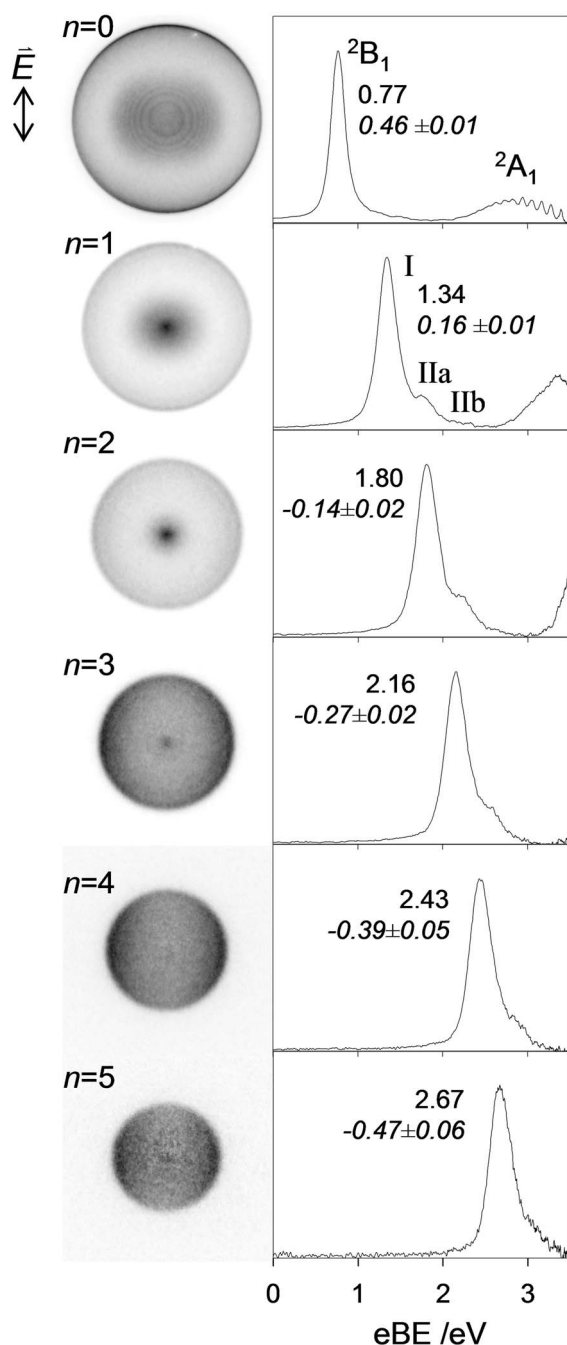


FIG. 3. Photoelectron images and energy spectra for photodetachment from $\text{NH}_2^-(\text{NH}_3)_n$, $n = 0-5$, at 355 nm. Image intensities are arbitrarily scaled; spectra are scaled to match peak intensities. Peak binding energies (in plain type, with ± 0.02 eV uncertainty) and anisotropy parameters (in italics) are indicated for the dominant transition. See text for details.

effects. Second, for $n = 5$, there is a sharp spike in intensity near the high-eBE or zero-eKE cutoff, which we assign as a new feature, labeled III.

B. Photoelectron spectra for $\text{NH}_2^-(\text{NH}_3)_n$, $n = 0-5$

Figure 3 displays the 355 nm photoelectron images and energy spectra for $\text{NH}_2^-(\text{NH}_3)_n$, $n = 0-5$. The 355 nm spectrum for unsolvated NH_2^- ($n = 0$) contains two bands. The

lowest binding energy transition (peaking at 0.77 eV) is assigned to removal of an electron from the b_1 HOMO of NH_2^- to generate the neutral amidogen radical in its 2B_1 ground state, as previously identified.^{30,39} The narrow width of this transition (labeled 2B_1 in Figure 3) and lack of vibrational progression are consistent with the small geometry change between the ground states of the anion and the neutral.⁴⁰⁻⁴²

The second, higher-eBE transition in the 355 nm photoelectron spectrum for NH_2^- (labeled 2A_1 in Figure 3) is attributed to removal of an electron from the a_1 HOMO-1 of the anion, yielding the A^2A_1 state of the neutral.⁴³ The band's onset is higher in binding energy than the peak of the 2B_1 transition by about 1.35 eV, a spacing closely matching the energy difference reported between the ground and first excited states of neutral amidogen (≈ 1.38 eV).⁴⁴ The peak spacing observed within this partially resolved band, ≈ 970 cm^{-1} , is consistent with the reported⁴⁴ bending mode interval (≈ 1000 cm^{-1}) in the A^2A_1 state of neutral NH_2 . The large extent of the observed vibrational progression indicates a significant geometry change along the bending coordinate between the X^1A_1 state of the anion and the A^2A_1 state of the neutral (and thus also between the A^2A_1 and X^2B_1 states of the neutral).

Both NH_2^- features persist in the spectrum for $n = 1$ in Figure 3, shifted to higher binding energies and somewhat broadened. The ground-state band is labeled I, while the additional features, labeled IIa and IIb, respectively reflect activation of one and two NH_3 vibrational quanta, as first identified by the Bowen group³⁰ and analogous to the similar bands observed for $\text{OH}^-(\text{NH}_3)_n$, $n = 1$ and 2.^{28,29,45} These features persist in the spectra of Figure 3 as n increases until clipped or suppressed at or near the energetic cutoff ($h\nu = 3.49$ eV).

The 532 nm results for $\text{NH}_2^-(\text{NH}_3)_n$, $n = 0-5$ are displayed in Figure 4. The spectrum for unsolvated NH_2^- is similar to that obtained at 355 nm, but here the photon energy is only sufficient to catch the onset of the transition accessing the 2A_1 excited state of the neutral. For $n = 1$, only type I and IIa features are seen; transition IIb is not apparent for the smaller photon energy, presumably due to proximity to threshold. The 532 nm spectrum for $n = 2$ contains two features analogous to those of the $n = 1$ spectrum but shifted to higher binding energies. In addition, a sharp spike is observed near the high-eBE/zero-eKE cutoff which appears to be distinct from feature II. This spike (labeled as a type-III feature) persists through $n = 5$, while direct one-photon detachment of the cluster becomes energetically inaccessible. Because analogous features are absent from the 355 nm spectra, we conclude that the type III features are not the result of direct photodetachment.

The $n = 4$ spectrum in Figure 4 contains two additional, weak features, labeled IV and V, respectively appearing at roughly the same binding energies as the X^2B_1 band for NH_2^- and band I for $\text{NH}_2^-(\text{NH}_3)$. Feature V may also be present (at the same eBE) for $n = 5$ (see the magnified portion of the spectrum in Figure 4). The $n = 4, 5$ photoelectron images in Figure 4 are shown in split scale to emphasize features IV and V.

To examine the nature of transitions III, IV, and V, the 532 nm image collection for $\text{NH}_2^-(\text{NH}_3)_n$, $n = 2-4$ was

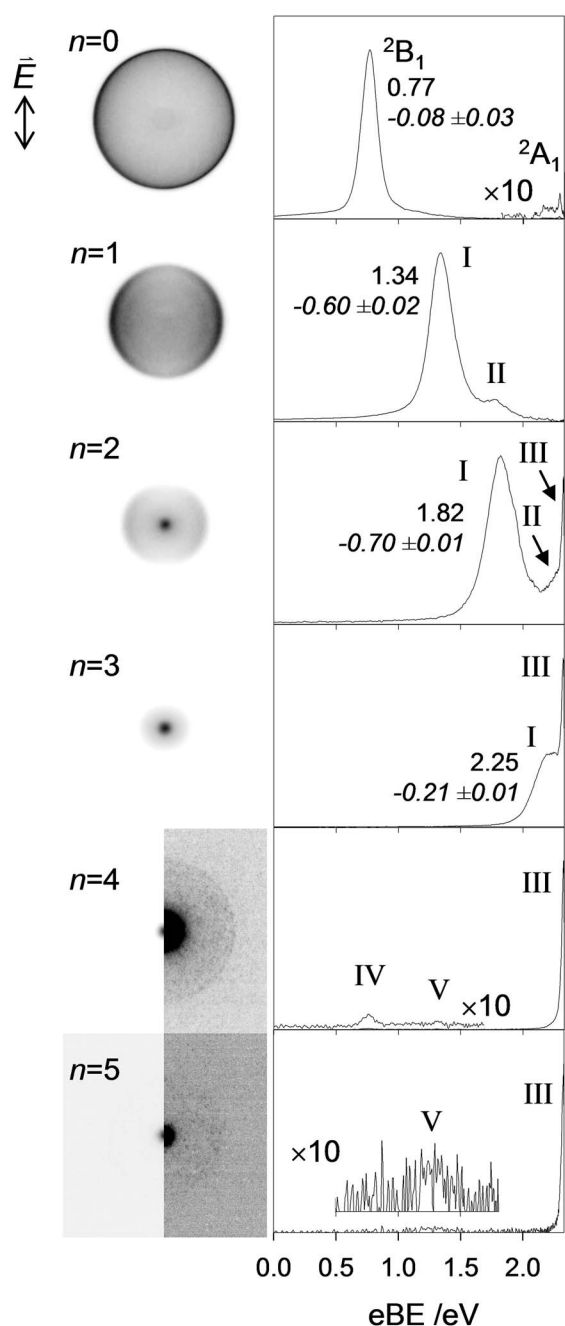


FIG. 4. Photoelectron images and energy spectra for photodetachment from $\text{NH}_2^-(\text{NH}_3)_n$, $n = 0-5$, at 532 nm. Image intensities are arbitrarily scaled; those for $n = 4$ and 5 are shown in split scale to emphasize the less intense features. Spectra are scaled for matching peak intensities, with details for $n = 0, 4, 5$ enhanced by a factor of ten. Peak binding energies (in plain type, with ± 0.02 eV uncertainty) and anisotropy parameters (in *italics*) are indicated for the dominant transition. See text for details.

repeated at twice the laser fluence. This resulted in no change in the relative intensities of bands I and III in the spectra for $n = 2$ and 3, indicating that feature III is not the result of a two-photon process. On the other hand, for $n = 4$, the intensities of bands IV and V approximately doubled relative to that of band I, indicating that peaks IV and V are the result of a two-photon process.

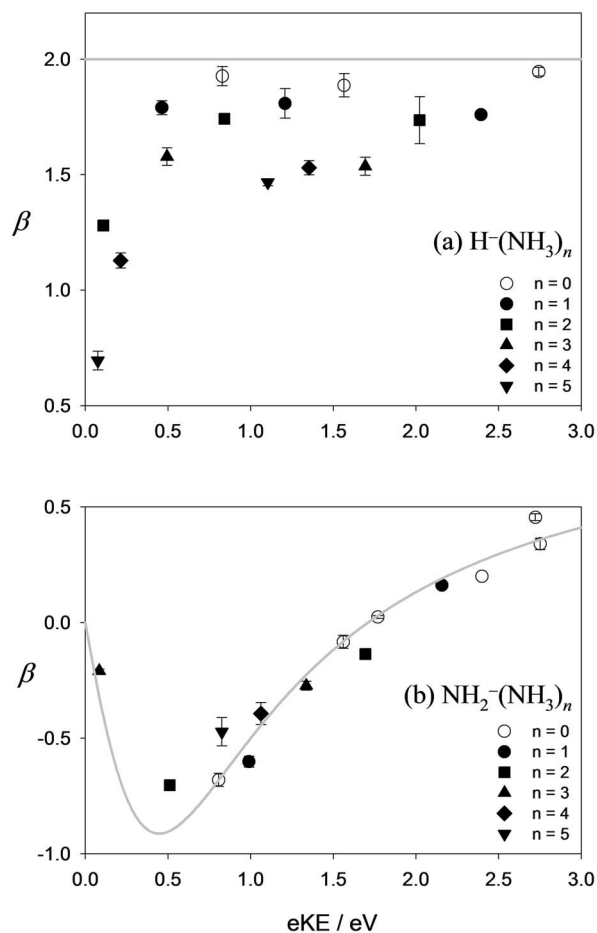


FIG. 5. (a) Average anisotropy parameters for $\text{H}^-(\text{NH}_3)_n$ at 532 nm ($n = 0-5$), 355 nm ($n = 0-5$), and 786 nm ($n = 0-2$). The grey line at $\beta = 2$ corresponds to the Wigner-Bethe-Cooper-Zare (WBCZ) prediction for bare H^- , according to Eq. (2) with $\ell_i = 0$. (b) Average anisotropy parameters for $\text{NH}_2^-(\text{NH}_3)_n$ at 532 nm ($n = 0-5$), 355 nm ($n = 0-5$) and 786 nm ($n = 0$). Two data points from other studies on bare NH_2^- are also included. The WBCZ model fit for photodetachment from bare NH_2^- , using Eq. (2) with $\ell_i = 1$, is plotted as a grey curve. Error bars correspond to \pm one standard deviation.

C. Photoelectron angular distributions

Photoelectron anisotropy parameters were computed over the full width at half-maximum (FWHM) of all lowest-eBE (type I) transitions, with the exception of those for $\text{H}^-(\text{NH}_3)_5$ and $\text{NH}_2^-(\text{NH}_3)_3$ at 532 nm, for which β was calculated over the lower-eBE halves of the transitions to minimize the contribution from overlapping bands. The β values reported in Figures 1-4 represent averages over the multiple images obtained for each species at each wavelength studied.

The average anisotropy parameters for $\text{H}^-(\text{NH}_3)_n$ and $\text{NH}_2^-(\text{NH}_3)_n$, $n = 0-5$ are plotted vs. eKE in Figures 5(a) and 5(b), respectively. The plots also include anisotropy values we obtained for 786 nm and 390 nm photodetachment of NH_2^- and 786 nm photodetachment of $\text{H}^-(\text{NH}_3)_n$, $n = 0-2$. (The photoelectron spectra from these measurements are consistent with the 355 nm results for these species and are not included here.) In addition, anisotropy parameters reported elsewhere for 488 nm photodetachment³⁹ and 532 nm photodetachment⁴¹ of NH_2^- are also included in Figure 5(b).

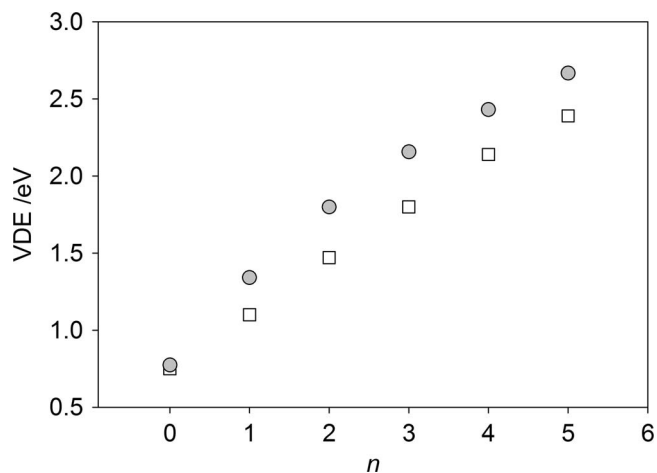


FIG. 6. Vertical detachment energies (determined as peak binding energies of the corresponding photoelectron bands) versus n for $\text{H}^-(\text{NH}_3)_n$ (open squares) and $\text{NH}_2^-(\text{NH}_3)_n$ (grey filled circles). Values are from 355 nm results.

IV. DISCUSSION

A. Photoelectron spectra

$\text{H}^-(\text{NH}_3)_n$ and $\text{NH}_2^-(\text{NH}_3)_n$, $n = 1$ and 2 , have been previously studied using photoelectron spectroscopy.^{28–30} Our work extends these studies to a larger cluster-size range ($n = 0–5$) and reveals several previously unobserved features. The type I and II direct photodetachment transitions in the spectra in Figures 1–4 are consistent with those observed by the Bowen group for $\text{H}^-(\text{NH}_3)_n$ and $\text{NH}_2^-(\text{NH}_3)_n$, $n = 1$ and 2 only.^{28–30} These bands are attributed to photodetachment from the anionic solute (H^- or NH_2^-) solvated by ammonia molecules. The cluster-size dependence of the VDEs (determined, approximately, from peak binding energies of type-I bands in the corresponding 355 nm spectra) is summarized in Figure 6. The plot for $\text{NH}_2^-(\text{NH}_3)_n$, shows a consistently greater slope than that for the H^- -based clusters, indicating that NH_2^- is stabilized by ammoniation to a greater degree than H^- for all degrees of solvation examined.

Type III features appear near zero eKE in the 532 nm energy spectra for $\text{NH}_2^-(\text{NH}_3)_n$, $n = 2–5$, and $\text{H}^-(\text{NH}_3)_5$. Of these species, a photoelectron spectrum was previously reported only for $\text{NH}_2^-(\text{NH}_3)_2$ (at 488 nm).³⁰ However, the instrumental low-eKE cutoff at about 0.2 eV inhibited observation of similar type III features in that work. The sharp type III bands observed in our work are essentially identical on the eKE scale, regardless of the cluster for which they are observed. The laser-power dependence of the intensity of these bands is indistinguishable from that of type I features, indicating their single-photon origin.

In addition, the type III features appear only when the photodetachment threshold for the given cluster is close to the photon energy. This condition is similar to that reported by the Neumark group for generation of weakly bound charge-transfer-to-solvent (CTTS) precursor states in $\text{I}^-(\text{NH}_3)_n$, $n = 4–15$,^{31,32} analogous to the clusters in the present study. These researchers monitored the temporal evolution of the

CTTS states via pump-probe photoelectron spectroscopy, observing increases in VDE on timescales of picoseconds, and decreases in signal intensity on timescales from 12 to 53 ps. While no autodetachment was directly observed (presumably due to the low-eKE cutoff of the detector), it was viewed as the most likely relaxation mechanism, due to the lack of fragmentation products.³¹ We find it likely that the type III features we observe upon 532 nm irradiation of $\text{NH}_2^-(\text{NH}_3)_n$, $n = 2–5$, and $\text{H}^-(\text{NH}_3)_5$ are due to autodetachment from analogous photoinduced CTTS states. Another possible explanation would be an enhancement in the near-threshold direct photodetachment cross-section due to significant long-range electron-neutral interactions, particularly due to the polar nature of the ammonia solvent.^{20,46} However, the overall pattern in appearance of these bands is less consistent with this explanation; thus, we favor the CTTS hypothesis.

Features IV and V in the 532 nm spectrum for $\text{NH}_2^-(\text{NH}_3)_4$ are the result of a two-photon process, as indicated by their quadratic laser-power dependence. These features peak at binding energies very similar to those of the $^2\text{B}_1$ band in the spectrum for NH_2^- and band I in the spectrum for $\text{NH}_2^-(\text{NH}_3)$, respectively (see Figure 4). We therefore believe that these signals are due to direct photodetachment from the NH_2^- and $\text{NH}_2^-(\text{NH}_3)$ fragment ions, generated as photoproducts of $\text{NH}_2^-(\text{NH}_3)_4$.

Photoexcitation to yield a metastable CTTS state is also a straightforward explanation for this fragmentation process, resulting in bands IV and V, as well as the autodetachment believed responsible for bands III. Specifically, absorption of one 532 nm photon (2.33 eV) by $\text{NH}_2^-(\text{NH}_3)_n$, $n = 2–5$, and $\text{H}^-(\text{NH}_3)_5$ may result in a transfer of the excess charge to the solvent network, followed either by (1) electron autodetachment (i.e., band III) or (2) charge back-transfer to regenerate the core anion, with the excess energy released via evaporation of three or four ammonia molecules. In case (2), absorption of a second photon by the photofragments would result in photodetachment from NH_2^- or $\text{NH}_2^-(\text{NH}_3)$ (i.e., bands IV and V).

B. Photoelectron angular distributions

As discussed in the Introduction, solvation of anions shifts the photodetachment bands to greater eBEs (smaller eKEs), thus affecting the relative partial-wave cross-sections and resulting in a general change in β . This shift is expected to manifest even in the absence of any change in the shape of the anion's orbitals or the photoelectron-solvent interactions. Therefore, for a meaningful examination of the electronic-structure or photoelectron-solvent interaction effects, one should compare the change in the $\beta(\text{eKE})$ trends for solvated vs. unsolvated anions, rather than single β values obtained at a given wavelength.²⁵ For atomic anions, the anisotropy parameter is described by the Bethe-Cooper-Zare central-potential model.^{8,15,16,47} Using this model with some additional assumptions, including the Wigner-law²⁰ scaling of the relative partial-wave cross-sections, β in atomic-anion photodetachment can be expressed as an explicit analytical function of eKE.⁴⁸

$$\beta = \frac{\ell_i(\ell_i - 1) + (\ell_i + 1)(\ell_i + 2)A^2\varepsilon^2 - 6\ell_i(\ell_i + 1)A\varepsilon \cos(\delta_{\ell_i+1} - \delta_{\ell_i-1})}{(2\ell_i + 1)[\ell_i + (\ell_i + 1)A^2\varepsilon^2]}, \quad (2)$$

where $\varepsilon \equiv e\text{KE}$, A is a constant reflecting the relative scaling of the partial-wave cross-sections, typically varied to fit experimental data, and $\delta_{\ell_i \pm 1}$ are the phase shifts of the corresponding dipole-allowed partial waves induced by their interaction with the remaining neutral. This equation may also be used for molecular anions, when the parent orbital is similar to an atomic-like orbital, by assigning it an effective orbital angular momentum quantum number.^{8,49}

In the case of detachment from an s orbital ($\ell_i = 0$), such as for H^- , electric-dipole selection rules predict the outgoing electron to be a p wave ($\ell = 1$). According to Eq. (2) with $\ell_i = 0$, $\beta = 2$ and is independent of eKE. This is a cosine-squared angular distribution with respect to the laser polarization axis (z), the same angular distribution as a p_z orbital.^{11,14}

The $\beta = 2$ limit serves as a theoretical zero-solvation reference for the $\text{H}^-(\text{NH}_3)_n$ cluster series. It is indicated in Figure 5(a) by a grey line. Our experimental results for bare H^- , plotted in the same figure as open circles, fall close to this limit and indeed do not display a striking energy dependence, consistent with other reported measurements for this system.^{50,51} In comparison, the $\text{H}^-(\text{NH}_3)_n$, $n > 0$ results, shown in Figure 5(a) as filled symbols, do exhibit significant deviations from the $\beta = 2$ limit. These solvation-induced deviations are most pronounced near zero eKE.

In contrast, photoelectron angular distributions for bare NH_2^- are strongly energy dependent. The β values corresponding to the X^2B_1 band are shown in Figure 5(b) as open circles. Because the b_1 HOMO of NH_2^- is essentially a nonbonding nitrogen p orbital, NH_2^- photodetachment may be modeled using Eq. (2) with $\ell_i = 1$.⁴¹ The Wigner-Bethe-Cooper-Zare model fit to the data for bare NH_2^- , with $A = 1.09 \text{ eV}^{-1}$ and $\cos(\delta_2 - \delta_0) = 0.934$, is plotted in Figure 5(b) (grey line) to serve as a zero-solvation reference for the $\text{NH}_2^-(\text{NH}_3)_n$ cluster series. Because the neutral species has a significant dipole moment (1.79 D),⁵² the energy-dependence of partial wave cross-sections may deviate from the Wigner law approximation,^{20,46} however, the model nonetheless works well here, as it has for other species whose neutrals have dipole moments even larger than 2 D.²³

The angular distributions for ammoniated NH_2^- (filled symbols in Figure 5b) show only minor deviations from the zero-solvation limit that are neither consistent in direction nor remarkable in magnitude, in contrast to the significant deviations observed for ammoniated H^- . This suggests that solvation has additional effect on PADs for solvated H^- that does not manifest considerably for solvated NH_2^- . As the solvent is the same in both cluster series, we conclude that the manifestation of solvent-induced deviations in $\beta(\text{eKE})$ depend strongly on the nature of the parent orbital. Because ammonia has both a large dipole moment (which should perturb the anion electronic structure) and a propensity to scatter low-energy electrons⁵³ (which should perturb photoelectron waves), both pre- and post-detachment solvent-electron

interactions are expected to affect the photoelectron angular distributions for $\text{H}^-(\text{NH}_3)_n$ and $\text{NH}_2^-(\text{NH}_3)_n$ to some extent. At present, we cannot rule out either effect for either system. However, we propose a relatively simple description for how solvation effects on parent orbital symmetry may manifest to different degrees in PADs, depending on the nature of the parent orbital of the solute.

Stronger solvent-solute interactions should logically result in larger perturbations of the solute's parent orbital. We may intuitively expect this to translate to larger deviations in PADs. The fact that solvation has a stronger effect on PADs for ammoniated H^- than for ammoniated NH_2^- is thus at first counterintuitive, considering that NH_3 molecules interact more strongly with NH_2^- than with H^- , as indicated by the respective shifts in vertical detachment energies across the two solvation series (see Figure 6).

On the other hand, we may consider the effects of solvation on the symmetry of the specific orbitals. Solvation of an s orbital (i.e., the parent orbital of H^-) should polarize the orbital, which can be thought of as introducing some p character to the initial state. Such polarization will result in the opening of the $\ell = 0$ photodetachment channel. Even if the perturbation is small, $\ell = 0$ waves are most important at small to moderate eKE,^{20,54} the region where the $\text{H}^-(\text{NH}_3)_n$ PADs deviate most strongly from the zero-solvation limit. On the other hand, in the photodetachment from a p orbital, the $\ell = 0$ channel is already open. Solvent-induced perturbation of a p state will add s, d, ... (etc.) character to the initial wavefunction, thus opening the $\ell = 1$ photodetachment channel. While the photoelectron anisotropy will be affected, the change is expected to be less significant than in the above perturbed s-orbital case, since the newly introduced $\ell = 1$ channel does not compete as favorably with the dominant $\ell = 0$ waves near the detachment threshold. Quantitative modeling of this effect is the subject of the accompanying paper.⁵⁵

V. CONCLUSIONS

We have reported 532 nm and 355 nm photoelectron imaging results for the $\text{H}^-(\text{NH}_3)_n$ and $\text{NH}_2^-(\text{NH}_3)_n$ ($n = 0-5$) cluster anions. The photoelectron spectra indicate that both cluster series may be described as the H^- or NH_2^- core anions electrostatically bound to NH_3 solvent molecules. The shifts in vertical detachment energies across the two series indicate that, for a given number of solvent molecules, the NH_2^- anion is solvated more strongly by ammonia, compared to H^- , while the photoelectron angular distributions reveal an opposite trend. Namely, the angular distributions for the $\text{H}^-(\text{NH}_3)_n$ series are found to deviate significantly from the zero-solvation (i.e., H^-) limit, while the corresponding deviations for $\text{NH}_2^-(\text{NH}_3)_n$, relative to bare NH_2^- , are minimal. These observations suggest that an anisotropic solvation environment may have a more pronounced effect on

photoelectron angular distributions emanating from predominantly s-character states. Further studies of photodetachment from simple orbitals in the vicinity of different solvents will be valuable to unraveling the environmental effects on photoelectron angular distributions through both the perturbation of the initial state and photoelectron-solvent interactions.

In addition, new features suggestive of autodetachment from metastable CTTS states are observed in the 532 nm photoelectron spectra of $\text{NH}_2^-(\text{NH}_3)_n$, $n = 2-5$ and $\text{H}^-(\text{NH}_3)_5$. The 532 nm spectrum of $\text{NH}_2^-(\text{NH}_3)_n$, $n = 4$ and 5 , also contains two-photon features assigned to detachment from the NH_2^- and $\text{NH}_2^-(\text{NH}_3)$ photofragments, likely generated via charge back-transfer from the same CTTS states.

ACKNOWLEDGMENTS

We thank Kostyantyn Pichugin for assistance with experiments at early stages of this project and comments on the manuscript prior to publication. This work is supported by the U.S. National Science Foundation (Grant CHE-1011895).

- ¹J. H. D. Eland, *Photoelectron Spectroscopy: An Introduction to Ultraviolet Photoelectron Spectroscopy in the Gas Phase* (Butterworths, London, 1984).
- ²K. M. Ervin and W. C. Lineberger, in *Advances in Gas Phase Ion Chemistry*, edited by N. G. Adams and L. M. Babcock (JAI, Greenwich, 1992), Vol. 1, pp. 121.
- ³A. Eppink and D. H. Parker, *Rev. Sci. Instrum.* **68**, 3477 (1997).
- ⁴D. W. Chandler and P. L. Houston, *J. Chem. Phys.* **87**, 1445 (1987).
- ⁵A. J. R. Heck and D. W. Chandler, *Annu. Rev. Phys. Chem.* **46**, 335 (1995).
- ⁶A. Osterwalder, M. J. Nee, J. Zhou, and D. M. Neumark, *J. Chem. Phys.* **121**, 6317 (2004).
- ⁷A. Sanov and R. Mabbs, *Int. Rev. Phys. Chem.* **27**, 53 (2008).
- ⁸J. Cooper and R. N. Zare, in *Atomic Collision Processes*, edited by S. Geltman, K. T. Mahanthappa, and W. E. Brittin (Gordon and Breach, New York, 1968), Vol. XI-C, pp. 317.
- ⁹J. G. Underwood and K. L. Reid, *J. Chem. Phys.* **113**, 1067 (2000).
- ¹⁰T. Seideman, *Annu. Rev. Phys. Chem.* **53**, 41 (2002).
- ¹¹R. Mabbs, E. R. Grumblin, K. Pichugin, and A. Sanov, *Chem. Soc. Rev.* **38**, 2169 (2009).
- ¹²A. W. Castleman and K. H. Bowen, *J. Phys. Chem.* **100**, 12911 (1996).
- ¹³A. Sanov and W. C. Lineberger, *Phys. Chem. Chem. Phys.* **6**, 2018 (2004).
- ¹⁴E. R. Grumblin, K. Pichugin, R. Mabbs, and A. Sanov, *J. Chem. Educ.* **88**, 1515 (2011).
- ¹⁵J. Cooper and R. N. Zare, *J. Chem. Phys.* **48**, 942 (1968).
- ¹⁶J. Cooper and R. N. Zare, *J. Chem. Phys.* **49**, 4252 (1968).
- ¹⁷K. L. Reid, *Annu. Rev. Phys. Chem.* **54**, 397 (2003).
- ¹⁸E. Surber, R. Mabbs, and A. Sanov, *J. Phys. Chem. A* **107**, 8215 (2003).
- ¹⁹C. M. Oana and A. I. Krylov, *J. Chem. Phys.* **127**, 234106 (2007).
- ²⁰E. P. Wigner, *Phys. Rev.* **73**, 1002 (1948).
- ²¹W. C. Lineberger, H. Hotop, and T. A. Patterson, in *Electron and Photon Interactions with Atoms*, edited by H. Kleinpoppen and M. R. C. McDowell (Plenum, New York, 1976), pp. 125.
- ²²R. D. Mead, K. R. Lykke, and W. C. Lineberger, in *Electronic and Atomic Collisions*, edited by J. Eichler, I. V. Hertel, and N. Stolterfoht (Elsevier, 1984), pp. 721.
- ²³R. Mabbs, E. Surber, and A. Sanov, *J. Chem. Phys.* **122**, 054308 (2005).
- ²⁴L. Velarde, T. Habteyes, E. R. Grumblin, K. Pichugin, and A. Sanov, *J. Chem. Phys.* **127**, 084302 (2007).
- ²⁵E. R. Grumblin, K. Pichugin, L. Velarde, and A. Sanov, *J. Phys. Chem. A* **114**, 1367 (2010).
- ²⁶M. Van Duzor, J. Wei, F. Mbaiwa, and R. Mabbs, *J. Chem. Phys.* **131**, 204306 (2009).
- ²⁷M. Van Duzor, J. Wei, F. Mbaiwa, and R. Mabbs, *J. Chem. Phys.* **133**, 144303 (2010).
- ²⁸J. V. Coe, J. T. Snodgrass, C. B. Friedhoff, K. M. McHugh, and K. H. Bowen, *J. Chem. Phys.* **83**, 3169 (1985).
- ²⁹J. T. Snodgrass, J. V. Coe, C. B. Friedhoff, K. M. McHugh, and K. H. Bowen, *Faraday Discuss.* **86**, 241 (1988).
- ³⁰J. T. Snodgrass, J. V. Coe, C. B. Friedhoff, K. M. McHugh, S. T. Arnold, and K. H. Bowen, *J. Phys. Chem.* **99**, 9675 (1995).
- ³¹C. Frischkorn, M. T. Zanni, A. V. Davis, and D. M. Neumark, *Faraday Discuss.* **115**, 49 (2000).
- ³²A. V. Davis, M. T. Zanni, C. Frischkorn, and D. M. Neumark, *J. Electron Spectrosc. Relat. Phenom.* **108**, 203 (2000).
- ³³R. Mabbs, E. Surber, and A. Sanov, *Analyst* **128**, 765 (2003).
- ³⁴M. A. Johnson and W. C. Lineberger, in *Techniques for the Study of Ion Molecule Reactions*, edited by J. M. Farrar and W. H. Saunders (Wiley, New York, 1988), pp. 591.
- ³⁵W. C. Wiley and I. H. McLaren, *Rev. Sci. Instrum.* **26**, 1150 (1955).
- ³⁶E. Surber, S. P. Ananthavel, and A. Sanov, *J. Chem. Phys.* **116**, 1920 (2002).
- ³⁷V. Dribinski, A. Ossadtchi, V. A. Mandelshtam, and H. Reisler, *Rev. Sci. Instrum.* **73**, 2634 (2002).
- ³⁸K. R. Lykke, K. K. Murray, and W. C. Lineberger, *Phys. Rev. A* **43**, 6104 (1991).
- ³⁹R. J. Celotta, R. A. Bennett, and J. L. Hall, *J. Chem. Phys.* **60**, 1740 (1974).
- ⁴⁰S. Roszak, *J. Chem. Phys.* **105**, 7569 (1996).
- ⁴¹C. T. Wickham-Jones, K. M. Ervin, G. B. Ellison, and W. C. Lineberger, *J. Chem. Phys.* **91**, 2762 (1989).
- ⁴²L. M. Tack, N. H. Rosenbaum, J. C. Owrutsky, and R. J. Saykally, *J. Chem. Phys.* **85**, 4222 (1986).
- ⁴³H. G. Herzberg, *Molecular Spectra and Molecular Structure III. Electronic Spectra and Electronic Structure of Polyatomic Molecules*. (Van Nostrand Reinhold, New York, 1966).
- ⁴⁴I. H. Bachir, T. R. Huet, J. L. Destombes, and M. Vervloet, *J. Mol. Spectrosc.* **193**, 326 (1999).
- ⁴⁵R. L. Schwartz, G. E. Davico, J. B. Kim, and C. W. Lineberger, *J. Chem. Phys.* **112**, 4966 (2000).
- ⁴⁶T. F. O'Malley, *Phys. Rev.* **137**, A1668 (1965).
- ⁴⁷H. A. Bethe, *Handbuch der Physik* (Springer, Berlin, 1933), Vol. 24, pp. 483.
- ⁴⁸D. Hanstorp, C. Bengtsson, and D. J. Larson, *Phys. Rev. A* **40**, 670 (1989).
- ⁴⁹R. J. Celotta, R. A. Bennett, J. Levine, J. L. Hall, and M. W. Siegel, *Phys. Rev. A* **6**, 631 (1972).
- ⁵⁰J. L. Hall and M. W. Siegel, *J. Chem. Phys.* **48**, 943 (1968).
- ⁵¹R. Reichle, H. Helm, and I. Y. Kiyani, *Phys. Rev. Lett.* **87**, 243001 (2001).
- ⁵²P. Jensen, W. P. Kraemer, and P. R. Bunker, *Molecular Physics* **101**, 613 (2003).
- ⁵³D. T. Alle, R. J. Gulley, S. J. Buckman, and M. J. Brunger, *J. Phys. B-At. Mol. Opt. Phys.* **25**, 1533 (1992).
- ⁵⁴K. J. Reed, A. H. Zimmerman, H. C. Andersen, and J. I. Brauman, *J. Chem. Phys.* **64**, 1368 (1976).
- ⁵⁵E. Grumblin and A. Sanov, *J. Chem. Phys.* **135**, 164302 (2011).